Journal of Molecular Spectroscopy 391 (2023) 111737

Contents lists available at ScienceDirect

Journal of Molecular Spectroscopy

journal homepage: www.elsevier.com/locate/yjmsp

The 130–500 GHz rotational spectrum of 2-cyanopyrimidine

Houston H. Smith, Brian J. Esselman, Maria A. Zdanovskaia, R. Claude Woods *, Robert J. McMahon *

Department of Chemistry, University of Wisconsin–Madison, Madison, Wisconsin 53706, USA

ARTICLE INFO

Keywords:
Rotational spectroscopy
Vibrational spectroscopy
Coriolis coupling
Interstellar molecule
Astrochemistry

ABSTRACT

The rotational spectrum of 2-cyanopyrimidine has been obtained from 130 GHz to 500 GHz. Over 7500 vibrational ground-state transitions have been assigned and least-squares fit to partial octic, A- and S-reduced Hamiltonians with low error (σ_{fit} = 36 kHz). The two lowest-energy fundamental modes, the out-of-plane (ν_{18}) and in-plane (ν_{27}) nitrile bending modes, form a Coriolis-coupled dyad similar to the analogous fundamental states of other cyanoarenes. The coupled dyad was least-squares fit to a partial octic, A-reduced Hamiltonian (σ_{fit} = 47 kHz) with over 6700 transitions for each vibrational state, including transitions that are perturbed or involved in resonances, as well as symmetry-allowed nominal interstate transitions resulting from Coriolis coupling. The spectroscopic information from these transitions enabled the determination of a highly precise energy separation ($\Delta E_{18,27}$ = 38.9673191 (77) cm^{-1}) and six Coriolis-coupling coefficients (G_a, G_a^J, G_a^K, G_a^{JJ}, F_{bc}, and F_{bc}^K). The spectroscopic constants and transitions presented in this work provide the foundation for future radioastronomical searches for 2-cyanopyrimidine.

1. Introduction

There has been long-standing interest in elucidating the molecular composition of various extraterrestrial environments, with particular attention on aromatic compounds. The detection of benzene *via* infrared spectroscopy in proto-planetary nebula CRL 618 [1] was a catalyst to search for other aromatic molecules; the search for aromatic heterocycles, however, has been unsuccessful [2–5]. Pyrimidine is of particular interest as an astronomical target because its core is present in various biological and prebiotic molecules. These include thymine, uracil, cytosine, thiamine (vitamin B1), and alloxan, as well as various synthetic drugs [6]. Therefore, detection of pyrimidine in an extraterrestrial environment would signify detection of a biologically relevant molecule in a harsh, possibly prebiotic environment. Despite multiple attempts, there have been no reported interstellar detections of this molecule [2,5,7]. Radioastronomy, which relies on the population of the species in the source observed and on the intrinsic intensity of its rotational transitions due to its dipole moment, is the preferred method of detection because it is reasonably unambiguous in molecular identification. The inability to detect nonpolar or weakly polar aromatic molecules has led to attempts to detect simple derivatives of those molecules with nitrile substituents, which tend to bestow a large dipole moment. The larger dipole moment leads to a greater chance of detection by radioastronomy, which is illustrated by the prevalence of nitrile-containing molecules detected in the interstellar medium (ISM) [8,9]. Such attempts to detect nitrile-containing derivatives have been successful for benzonitrile [10] and cyanonaphthalenes [11], suggesting their parent molecules are also present in space. These astronomical detections rely on the availability of accurate spectroscopic constants determined from laboratory spectra. Given the success of nitrile-substituted detections, our group reported the rotational spectral analyses of several nitrile-containing aromatic and heteroaromatic compounds (Fig. 1), including benzonitrile [12,13], 2-cyanopyridine [14], 3-cyanopyridine [15], 4-cyanopyridine [16], cyanopyrazine [17], and 2-cyanopyrimidine (presented in this work) in their ground and vibrationally excited states. In contrast to the situation with benzonitrile and the cyanopyridines, for which some spectroscopic data had been previously available [18–21], 2-cyanopyrimidine and cyanopyrazine did not have previously reported rotational spectra.

The two lowest-energy vibrational modes for molecules containing a π-conjugated nitrile moiety are typically the in-plane and out-of-plane bending modes of the nitrile, and these modes are often sufficiently close in energy that Coriolis coupling is observed in the millimeter-wave frequency transitions. Analysis of the rotational spectra for these vibrational modes for benzonitrile [12,13], 3-cyanopyridine [15], 4-cyanopyridine [16], cyanopyrazine [17], 1-cyanocyclobutene [22],

* Corresponding authors.
E-mail addresses: rcwoods@wisc.edu (R.C. Woods), robert.mcmahon@wisc.edu (R.J. McMahon).

https://doi.org/10.1016/j.jms.2023.111737
Received 8 December 2022; Received in revised form 6 January 2023; Accepted 8 January 2023
Available online 10 January 2023
0022-2852/© 2023 Elsevier Inc. All rights reserved.

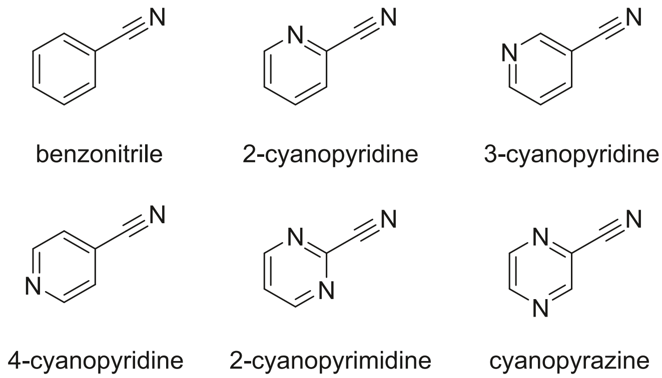

Fig. 1. Cyanoarenes derived from benzene, pyridine, pyrimidine, and pyrazine.

Table 1
Energy differences between out-of-plane and in-plane nitrile bending modes for molecules containing a π-conjugated nitrile moiety.

	out-of-plane	in-plane	ΔE_{ip-oop} (cm^{-1})
benzonitrile [12,13]	ν_{22}, B_1	ν_{33}, B_2	19.1081701(74)
3-cyanopyridine [15]	ν_{30}, A″	ν_{21}, A′	15.7524693 (37)
4-cyanopyridine [16]	ν_{20}, B_1	ν_{30}, B_2	18.806554 (11)
cyanopyrazine [17]	ν_{27}, A″	ν_{19}, A′	24.8245962 (60)
2-cyanopyrimidine (this work)	ν_{18}, B_1	ν_{27}, B_2	38.9673191 (77)
1-cyanocyclobutene [22]	ν_{27}, A″	ν_{17}, A′	14.0588093 (43)
(cyanomethylene)cyclopropane [23]	ν_{27}, A″	ν_{17}, A′	−29.8975453 (33)
acrylonitrile [24,25]	ν_{15}, A″	ν_{11}, A′	−104.378277 (6)

(cyanomethylene)cyclopropane [23], and acrylonitrile [24] required the use of vibrationally coupled Hamiltonians to assign the observed rotational transitions and resulted in the determination of highly accurate and precise energy separations between the two fundamental states (Table 1). For each of the cyano-substituted aromatic compounds observed, the out-of-plane nitrile bending mode is lower in energy (Table 1). The coupling and state mixing result in rotational transitions influenced by Coriolis perturbation. This perturbation results in the appearance of local resonances, *i.e.*, transitions whose frequencies are drastically shifted from where they would be expected in the absence of perturbation, and formally forbidden, nominal interstate transitions. While band origins can be determined from high-resolution infrared spectroscopy, as has been done for benzonitrile [13] and acrylonitrile [24], it is the various coupling interactions affecting the rotational transition frequencies that enable the highly precise determination of the energy separation between vibrational states. This work presents the rotational spectroscopy and analysis of the ground and two lowest-energy vibrationally excited states of 2-cyanopyrimidine from 130 GHz to 500 GHz.

2. Experimental methods

A commercial sample of 2-cyanopyrimidine (Oakwood, 99% purity) was used without further purification. Using a millimeter-wave spectrometer that has been previously described [26,27], the rotational spectrum of 2-cyanopyrimidine was collected from 130 to 230 and from 235 to 360 GHz in a continuous flow at room temperature, with a sample pressure of 3 mTorr. Additional spectral data were obtained with a newly acquired amplification and multiplication chain that extended the frequency range to 500 GHz with a sample pressure of 4 mTorr. The separate spectral segments were combined into a single broadband spectrum using Kisiel's Assignment and Analysis of Broadband Spectra (AABS) software [24,28]. The complete spectrum from 130 to 500 GHz was obtained using automated data collection software over approximately nine days given these experimental parameters: 0.6 MHz/sec sweep rate, 10 ms time constant, and 50 kHz AM and 500 kHz FM modulation in a tone-burst design [29]. Pickett's SPFIT/SPCAT programs [30] were used for least-squares fits and spectral predictions, along with Kisiel's PIFORM, PLANM, and AC programs for analysis [31,32]. A uniform frequency measurement uncertainty of 0.050 MHz was assumed for all measurements.

3. Computational methods

Electronic structure calculations were carried out with Gaussian 16 [33] using the WebMO interface [34] to obtain theoretical spectroscopic constants. Optimized geometries at the B3LYP/6–311+(2d,p) and MP2/6–311+(2d,p) levels were obtained using "verytight" convergence criteria and an "ultrafine" integration grid. Subsequent anharmonic

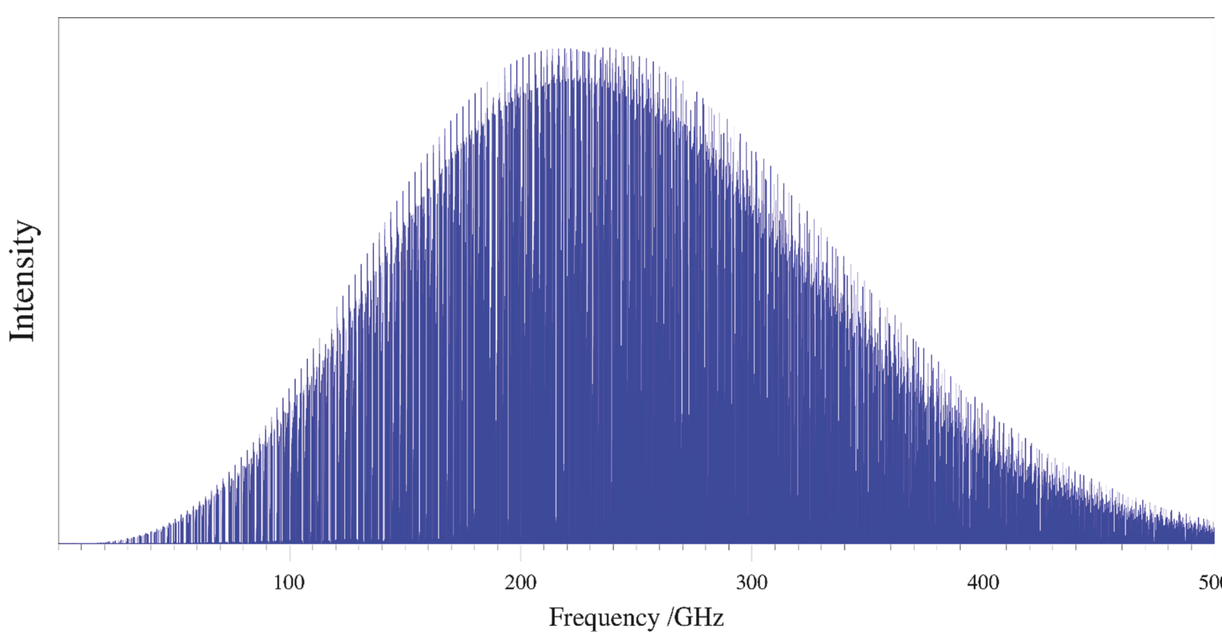

Fig. 2. Predicted rotational spectrum of the ground vibrational state of 2-cyanopyrimidine at 292 K.

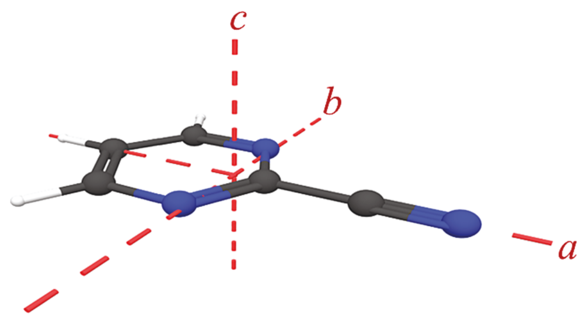

Fig. 3. 2-Cyanopyrimidine (C_{2v}, μ_a = 6.5 D, B3LYP) structure with principal inertial axes.

vibrational frequency calculations were carried out to obtain vibration–rotation interaction constants and predictions of the centrifugal distortion constants. These methods have been effective to generate the necessary spectroscopic constants for adequate *a priori* predictions for other cyanoarenes [12,13,15–17]. From the optimized geometries, magnetic calculations were also performed to obtain theoretical nuclear quadrupole coupling constants. Computational output files can be found in the supplementary material.

4. 2-Cyanopyrimidine rotational spectrum

The rotational spectrum of 2-cyanopyrimidine was obtained from 130 to 500 GHz. This frequency range satisfactorily covered the most intense rotational transitions, as judged by comparison to the predicted rotational populations in the 2-cyanopyrimidine spectrum at ambient temperature (Fig. 2). While the peak transition intensities occur near 220 GHz, there is still substantial intensity well beyond 400 GHz. As will be discussed below, this extension in the frequency range to 500 GHz was vital in the analysis of the Coriolis-coupled dyad of ν_{18} and ν_{27}, because most resonances were observed between 375 and 500 GHz, providing crucial coupling information.

4.1. Ground-State spectral analysis

The rotational spectrum of 2-cyanopyrimidine (μ = 6.5 D (B3LYP), κ = −0.851) has not been previously reported. As a consequence of C_{2v} symmetry and the nitrile substituent lying along the *a*-principal axis (Fig. 3), 2-cyanopyrimidine exhibits only *a*-type rotational transitions. The rotational spectrum of this prolate, asymmetric top is thus dominated by $^{a}R_{0,1}$ ground-state and vibrationally excited-state transitions across the frequency range studied. Fig. 4 shows a small subset of the spectrum from 198 GHz to 199 GHz along with predicted stick spectra for the ground state and the two lowest-energy vibrationally excited states, ν_{18} and ν_{27}. It is apparent that the spectrum also includes unassigned transitions that are due to higher-energy vibrationally excited states, but they are not addressed in this work. Similar to other mono-substituted arenes, despite being a near-prolate top (κ = −0.851), the most prominent band structure for the ground state of 2-cyanopyrimidine follows the recognizable oblate-type band pattern at low K_a [12,13,15–17,35]. Bands start at K_a = 0 and increase in K_a as J'' decreases. The band in Fig. 4 begins with a K_c-degenerate pair of $^{a}R_{0,1}$ transitions, which lose degeneracy at higher K_a values. The degenerate $^{a}R_{0,1}$ transitions have quantum numbers that follow either $K_a + K_c = J$ or $K_a + K_c = J + 1$, and K_a series with these selection rules are subsequently referred to as K_a^{+} and K_a^{-}, respectively.

The vibrational ground state of 2-cyanopyrimidine has been least-squares fit to partial octic A- and S-reduced, single-state Hamiltonians with low error (σ_{fit} = 36 kHz). As shown in Fig. 5, the final transition data set (~7600 transitions) encompasses an extensive range of quantum numbers with J'' + 1 = 42 to 189 and K_a = 0 to 63. The resulting spectroscopic constants are reported in Table 2 along with respective computed values (B3LYP and MP2). Though a partial octic Hamiltonian was utilized, no computational comparison is possible for the octic centrifugal distortion constants, because there is no readily available software to compute these values. As a result, octic terms that were undeterminable in the least-squares fit were set to a value of zero. There were an insufficient number of nuclear quadrupole coupling-resolved transitions to obtain experimental nuclear quadrupole coupling constants, therefore these terms were not included in the Hamiltonian. Least-squares fitting files and computed nuclear quadrupole coupling constants can be found in the supplementary material.

The MP2-computed rotational constants are in satisfactory agreement with the experimental values (within ~ 1%), but the B3LYP-computed rotational constants are closer in agreement (within ~ 0.13%). This result is similar to the situation observed for cyanopyrazine [17]. The B3LYP-computed quartic centrifugal distortion constants are also in good agreement with the experimental values (within 10%), with Δ_K and D_K having the largest difference from experiment. The MP2

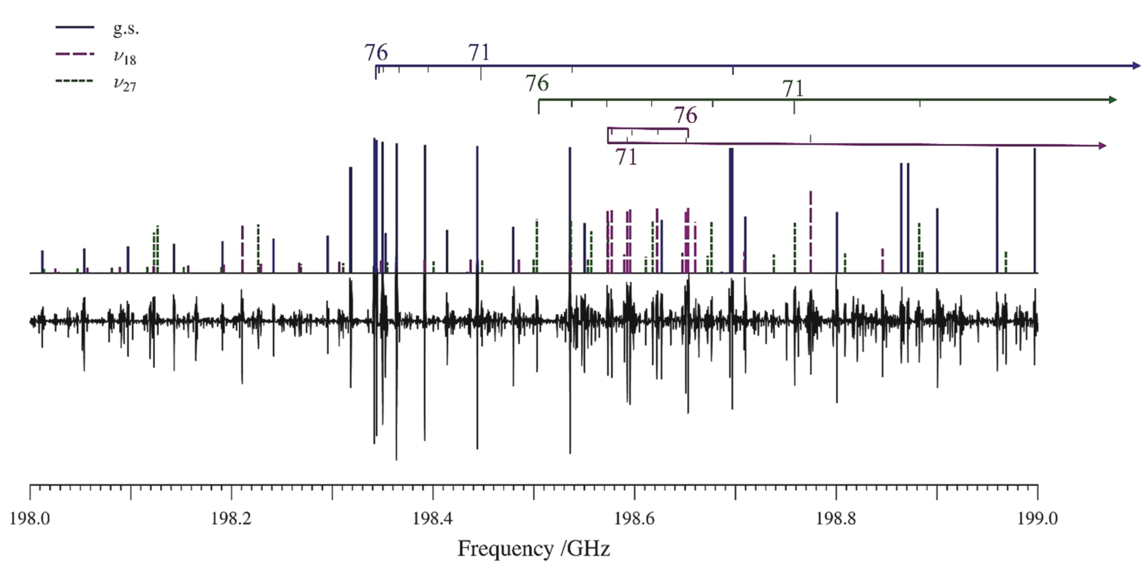

Fig. 4. Experimental rotational spectrum (bottom) of 2-cyanopyrimidine from 198 to 199 GHz and stick spectra (top) from experimental spectroscopic constants. The ground state (blue), ν_{18} (magenta), and ν_{27} (green) are labeled by the upper energy-level quantum number, J'' + 1. (For interpretation of the references to colour in this figure legend, the reader is referred to the web version of this article.)

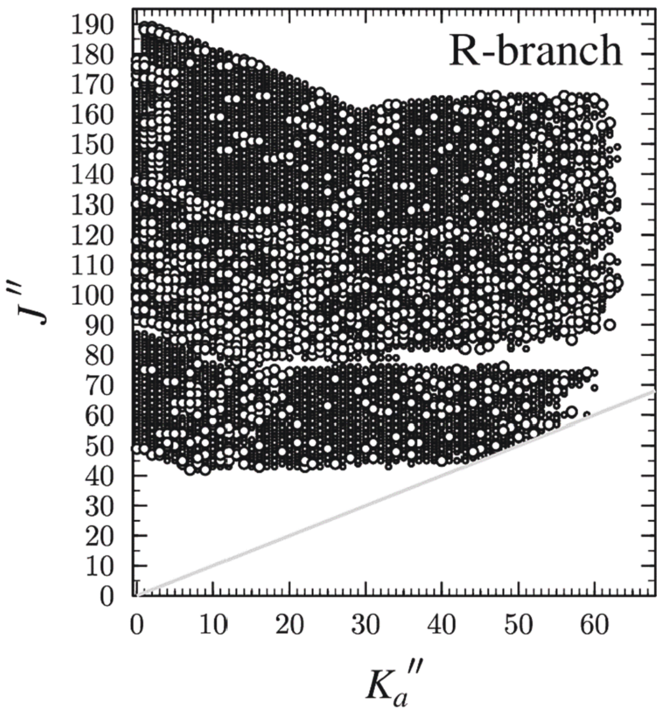

Fig. 5. Data distribution plot for the least-squares fit of spectroscopic data for the vibrational ground state of 2-cyanopyrimidine. The size of the outlined circle is proportional to the value of $|(f_{obs.} - f_{calc.})/\delta f|$, where δf is the frequency measurement uncertainty and all values are less than 3.

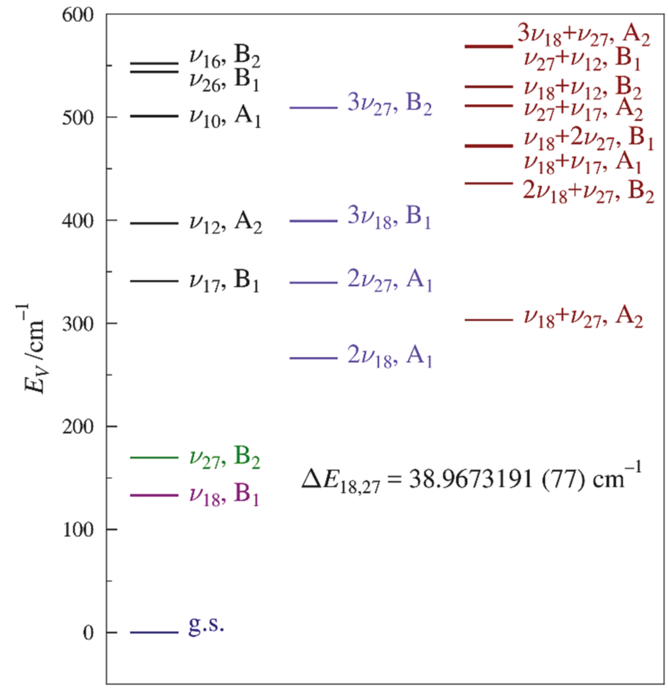

Fig. 6. Vibrational energy levels of 2-cyanopyrimidine below 600 cm^{-1} from computed fundamental frequencies (B3LYP/6–311+G(2d,p)). The value of $\Delta E_{18,27}$ results from the experimental perturbation analysis of ν_{18} and ν_{27} in this work (*vide infra*).

quartic centrifugal distortion constants are in slightly closer agreement with the experimental values (within 5%), with δ_J and d_1 having the largest discrepancies. There is poorer agreement for the sextic centrifugal distortion constants for both sets of computed values. With the exception of Φ_K and ϕ_J, the B3LYP values are within ~ 15%, and the MP2 values are within 10%, excluding H_K, and h_1. The B3LYP values of Φ_K and H_K are approximately half of their experimental values, and the MP2 values are only slightly closer. The values of ϕ_J and h_1 are the smallest of the sextic centrifugal distortion constants, so it is not surprising that their predictions have large relative errors. The worst of

Table 2
Experimental and computational spectroscopic constants for the ground vibrational state of 2-cyanopyrimidine (A- and S-reduced Hamiltonians, I^r representation).

	A Reduction, I^r representation				S Reduction, I^r representation		
	Experimental [a]	B3LYP [b]	MP2 [b]		Experimental [a]	B3LYP [b]	MP2 [b]
A_0 (MHz)	6043.4539 (12)	6051	5986	A_0 (MHz)	6043.4535 (12)	6051	5986
B_0 (MHz)	1651.140609 (36)	1649	1635	B_0 (MHz)	1651.139276 (36)	1649	1635
C_0 (MHz)	1296.639905 (39)	1295	1284	C_0 (MHz)	1296.641199 (39)	1295	1284
Δ_J (kHz)	0.0483056 (22)	0.0464	0.0460	D_J (kHz)	0.0354922 (20)	0.0345	0.0338
Δ_{JK} (kHz)	1.037502 (25)	0.976	1.01	D_{JK} (kHz)	1.114400 (26)	1.05	1.08
Δ_K (kHz)	0.3608 (18)	0.389	0.351	D_K (kHz)	0.3003 (18)	0.330	0.290
δ_J (kHz)	0.01154427 (86)	0.0111	0.0110	d_1 (kHz)	−0.01154436 (86)	−0.0111	−0.0110
δ_K (kHz)	0.660687 (56)	0.621	0.635	d_2 (kHz)	−0.00640999 (54)	−0.00594	−0.00611
Φ_J (Hz)	0.000001716 (84)	0.00000174	0.00000187	H_J (Hz)	−0.000012737 (77)	−0.0000117	−0.0000129
Φ_{JK} (Hz)	0.0017323 (24)	0.00149	0.00163	H_{JK} (Hz)	0.0011987 (19)	0.00103	0.00115
Φ_{KJ} (Hz)	−0.008505 (15)	−0.00739	−0.00819	H_{KJ} (Hz)	−0.006498 (16)	−0.00566	−0.00634
Φ_K (Hz)	0.0107 (10)	0.00653	0.00718	H_K (Hz)	0.0116 (10)	0.00528	0.00583
ϕ_J (Hz)	0.000001226 (19)	0.000000881	0.000000922	h_1 (Hz)	−0.000000239 (19)	−0.000000409	−0.00000046
ϕ_{JK} (Hz)	0.0008021 (15)	0.000751	0.000824	h_2 (Hz)	0.000007394 (15)	0.00000674	0.00000740
ϕ_K (Hz)	0.008258 (34)	0.00731	0.00779	h_3 (Hz)	0.0000014737 (48)	0.00000129	0.00000139
L_J (mHz)	0.0000000167 (12)			L_J (mHz)	0.0000000114 (12)		
L_{JJK} (mHz)	−0.000002409 (17)			L_{JJK} (mHz)	−0.000002025 (17)		
L_{JK} (mHz)	0.00001448 (22)			L_{JK} (mHz)	0.00001835 (22)		
L_{KKJ} (mHz)	−0.0001149 (31)			L_{KKJ} (mHz)	−0.0001301 (31)		
L_K (mHz)	[0.]			L_K (mHz)	[0.]		
Δ_i (uÅ^2) [c,d]	0.057658 (21)			Δ_i (uÅ^2) [c,d]	0.057568 (21)		
N_{lines} [e]	7591			N_{lines} [e]	7591		
σ_{fit} (MHz)	0.036			σ_{fit} (MHz)	0.036		

[a] Off-diagonal octic centrifugal distortion terms (not shown in table) were held constant at a value of zero.
[b] Evaluated with the 6–311+G(2d,p) basis set.
[c] Inertial defect, $\Delta_i = I_c - I_a - I_b$.
[d] Calculated using PLANM from the B_0 constants.
[e] Number of fitted transition frequencies.

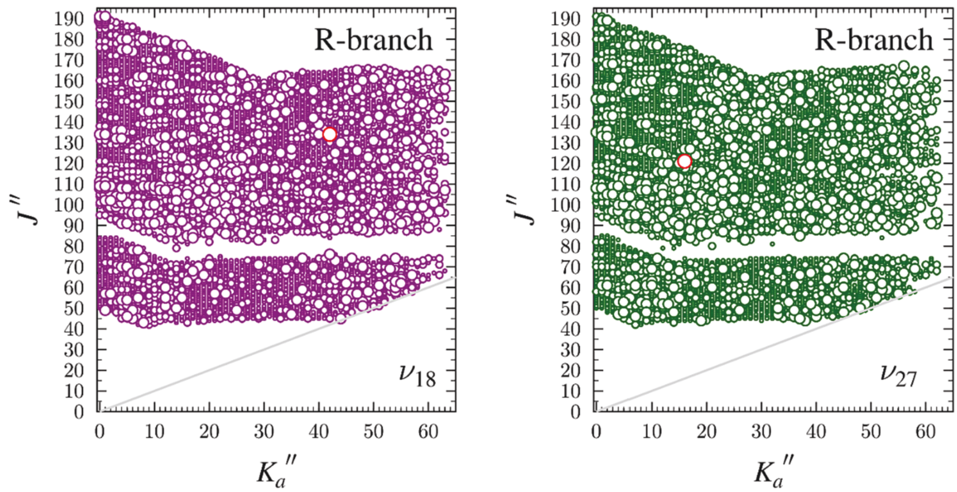

Fig. 7. Data distribution plots for the least-squares fit of spectroscopic data for the lowest-energy fundamental states of 2-cyanopyrimidine, ν_{18} (magenta) and ν_{27} (green). The size of the symbol is proportional to the value of $|(f_{obs.} - f_{calc.})/\delta f|$, where δf is the frequency measurement uncertainty, and values greater than 3 are depicted in red. (For interpretation of the references to colour in this figure legend, the reader is referred to the web version of this article.)

these, the MP2 prediction of h_1, is approximately twice the size of the experimental value. Unlike the case of cyanopyrazine [17], however, no sign change in the value of h_1 was observed for 2-cyanopyrimidine. On average, the MP2 computed distortion constants are in closer agreement with experiment than the B3LYP values. Despite the discrepancies described for each set of computed values, they provide very good *a priori* predictions of the rotational spectrum and are important in assisting the early stage of least-squares fitting.

4.2. Spectral analysis of ν_{18} and ν_{27}

The two lowest-energy vibrationally excited states of 2-cyanopyrimidine are an isolated, Coriolis-coupled dyad, similar to those seen in other cyanoarenes [12,13,15–17]. The lower-energy vibration, ν_{18} (B_1, 132 cm^{-1} B3LYP), is an out-of-plane bend of the nitrile group with respect to the aromatic ring, while ν_{27} (B_2, 175 cm^{-1} B3LYP) involves an in-plane bend of the nitrile group. The vibrational manifold of 2-cyanopyrimidine below 600 cm^{-1} is presented in Fig. 6, which depicts additional possible coupled states, especially above 450 cm^{-1}. This work focuses only on the coupled dyad of ν_{18} and ν_{27}. The initial assignment of ν_{18} and

Table 3
Experimentally determined spectroscopic constants for the ground and vibrationally excited states ν_{18} and ν_{27} of 2-cyanopyrimidine (A-reduced Hamiltonian, I^r representation).

	ground state [a]	ν_{18} (B_1, 133 cm^{-1}) [a,b]	ν_{27} (B_2, 175 cm^{-1}) [a,b]
A_v (MHz)	6043.4539 (12)	6051.08 (13)	6032.06 (13)
B_v (MHz)	1651.140609 (36)	1653.012774 (36)	1654.267680 (36)
C_v (MHz)	1296.639905 (39)	1298.754909 (32)	1297.555132 (34)
Δ_J (MHz)	0.0483056 (22)	0.0492650 (13)	0.0493417 (13)
Δ_{JK} (MHz)	1.037502 (25)	1.06773 (49)	0.98437 (49)
Δ_K (MHz)	0.3608 (18)	[0.3608]	0.4143 (13)
δ_J (MHz)	0.01154427 (86)	0.01162990 (85)	0.01194518 (88)
δ_K (MHz)	0.660687 (56)	0.663053 (60)	0.662360 (57)
Φ_J (MHz)	0.000001716 (84)	0.000002372 (31)	0.000002309 (31)
Φ_{JK} (MHz)	0.0017323 (24)	0.0017797 (84)	0.0016502 (88)
Φ_{KJ} (MHz)	−0.008505 (15)	−0.008081 (11)	[−0.008505]
Φ_K (MHz)	0.0107 (10)	[0.0107]	[0.0107]
ϕ_J (MHz)	0.000001226 (19)	0.000001384 (18)	0.000001592 (18)
ϕ_{JK} (MHz)	0.0008021 (15)	0.0008179 (11)	0.0007685 (11)
ϕ_K (MHz)	0.008258 (34)	0.008228 (26)	0.008475 (27)
$\Delta E_{18,27}$ (MHz)		1168210.84 (23)	
$\Delta E_{18,27}$ (cm^{-1})		38.9673191 (77)	
G_a (MHz)		10666.3 (75)	
G_a^J (MHz)		−0.006165 (29)	
G_a^K (MHz)		−0.00466 (14)	
G_a^{JJ} (MHz)		0.00000000635 (44)	
F_{bc} (MHz)		−0.3779 (26)	
F_{bc}^K (kHz)		−0.000006992 (97)	
Δ_i (uÅ^2) [c,d]	0.057658 (21)	−0.1214 (19)	0.1997 (19)
N_{lines} [e]	7591	7114	6712
σ_{fit} (MHz)	0.036	0.046	0.048

[a] Octic centrifugal distortion constants are not shown and, for the excited states, are held constant at their ground-state values in Table 2.
[b] Fundamental frequencies calculated using B3LYP/6–311+G(2d,p).
[c] Inertial defect, $\Delta_i = I_c - I_a - I_b$.
[d] Calculated using PLANM from the B_v constants.
[e] Number of fitted transition frequencies.

Table 4
Vibration-rotation interaction and Coriolis-coupling constants of the 2-cyano-pyrimidine ν_{18}-ν_{27} dyad.

	Experimental	B3LYP [a]	MP2 [a]
$A_0 - A_{18}$ (MHz)	−7.62 (13)	81.13	95.75
$B_0 - B_{18}$ (MHz)	−1.872165 (51)	−1.84	−1.77
$C_0 - C_{18}$ (MHz)	−2.115004 (50)	−2.09	−2.03
$A_0 - A_{27}$ (MHz)	11.39 (13)	−77.53	−92.33
$B_0 - B_{27}$ (MHz)	−3.127071 (51)	−2.96	−3.08
$C_0 - C_{27}$ (MHz)	−0.915227 (52)	−0.85	−0.91
$\frac{(A_0 - A_{18}) + (A_0 - A_{27})}{2}$(MHz)	1.88 (09)	1.80	1.71
$\frac{(B_0 - B_{18}) + (B_0 - B_{27})}{2}$(MHz)	−2.499618 (36)	−2.40	−2.43
$\frac{(C_0 - C_{18}) + (C_0 - C_{27})}{2}$(MHz)	−1.515115 (36)	−1.47	−1.47
$\lvert\zeta^a_{18,27}\rvert$	0.873	0.809	0.810
$\Delta E_{18,27}$ (cm^{-1})	38.9673191 (77)	42.70	36.64

[a] Evaluated with the 6–311+G(2d,p) basis set.

ν_{27} was performed using a single-state, distorted-rotor Hamiltonian for each vibrational state. Computationally predicted rotational constants and ground-state distortion constants were used for initial predictions. This technique allowed for the assignment of three series corresponding to $K_a = 0$, 1, and 2 for both states, but there was apparent perturbation in each least-squares fit that was untreated in a single-state model. Thus, a two-state model was adopted, initially using the $\Delta E_{18,27}$ and G_a values predicted by B3LYP and the rotational constants A_0, B_v and C_v (A_0 is the experimental ground-state value and B_v and C_v are the experimental ground-state values corrected by the respective B3LYP vibration–rotation interaction constants, α_B and α_C, for each vibrational state). The vibration–rotation interaction constant, α_A, was not used because it showed clear signs of absorbed perturbation (equal magnitude but opposite sign for each state; *vide infra*). Quartic, sextic, and octic distortion constants were set to their ground-state values, and in the initial least-squares fitting process, only ΔE and C_v were allowed to vary. As transitions were added to the least-squares fit, additional rotational, centrifugal, and Coriolis-coupling coefficients were varied to model the experimental spectrum until all observed transitions for each vibrational state were assigned across the frequency region measured. The extent of the rotational transitions measured is shown in Fig. 7, and the spectroscopic constants determined in the least-squares fit are provided in Table 3.

The final least-squares fit is an exhaustive collection of transitions across the frequency region and totals over 7100 transitions for ν_{18} and 6700 for ν_{27}. The totals are only slightly lower than that for the ground state (~7600), which is expected due to the somewhat lower intensity of vibrationally excited states. The observed transitions range from 42 to 192 in $J'' + 1$ for both states and $K_a = 0$ to 63 and 62 for ν_{18} and ν_{27}, respectively. The data set includes transition frequencies that are shifted *via* global perturbations and intense resonances and includes 17 transitions that are formally forbidden, coupling-allowed interstate transitions. To achieve a satisfactory fit, it was necessary to extend the frequency range beyond 360 GHz, because most resonances occur in this region. These highly perturbed resonant transitions are critical in determining accurate and precise Coriolis-coupling constants. The importance of data in the higher frequency region was noted in the earlier case of cyanopyrazine [17], and it is even more important for 2-cyanopyrimidine. Attempts to obtain a satisfactory least-squares fit using only data from the 130 GHz to 360 GHz frequency range were ultimately unsuccessful. Least-squares fitting of the final data set, including resonant transitions and symmetry-allowed interstate transitions, provides a precise energy separation between ν_{18} and ν_{27} ($\Delta E_{18,27}$ = 38.9673191 (77) cm^{-1}). Based on similar results in molecules where the band origins have been measured independently by high-resolution infrared spectroscopy [13], the accuracy is presumed to be comparable to the precision. This large energy separation required much higher values of J and K of ν_{18} before the energy levels are sufficiently close to create resonances than in some previous works with smaller energy separations between the coupled modes [12,13,15,16,35]. Along with a precise value of $\Delta E_{18,27}$, the least-squares fit provides a nearly complete set of quartic and sextic distortion constants, excluding Δ_K for ν_{18}, Φ_{KJ} for ν_{27} and Φ_K for both ν_{18} and ν_{27}. Unfortunately, Δ_K of ν_{18} could not be determined, which is attributed to the high correlation of Δ_K with A_{18} and the limitation of being able to measure only $^a\mathrm{R}_{0,1}$ transitions. In addition, six Coriolis-coupling terms (G_a, G_a^J, G_a^K, G_a^{JJ}, F_{bc}, and F_{bc}^K) were determined. The inclusion of all of these coupling terms was needed to obtain a satisfactory least-squares fit with a total error lower than the measurement uncertainty of 50 kHz.

A measure of the quality of the least-squares fit comes from the comparison of the computed rotational constants to those experimentally determined, to establish whether or not any of the computed constants show signs of untreated Coriolis coupling. The vibration–rotation interaction constants (Table 4) provide a straightforward comparison between the experimental and computed values, where unaddressed Coriolis coupling appears as large values with opposing

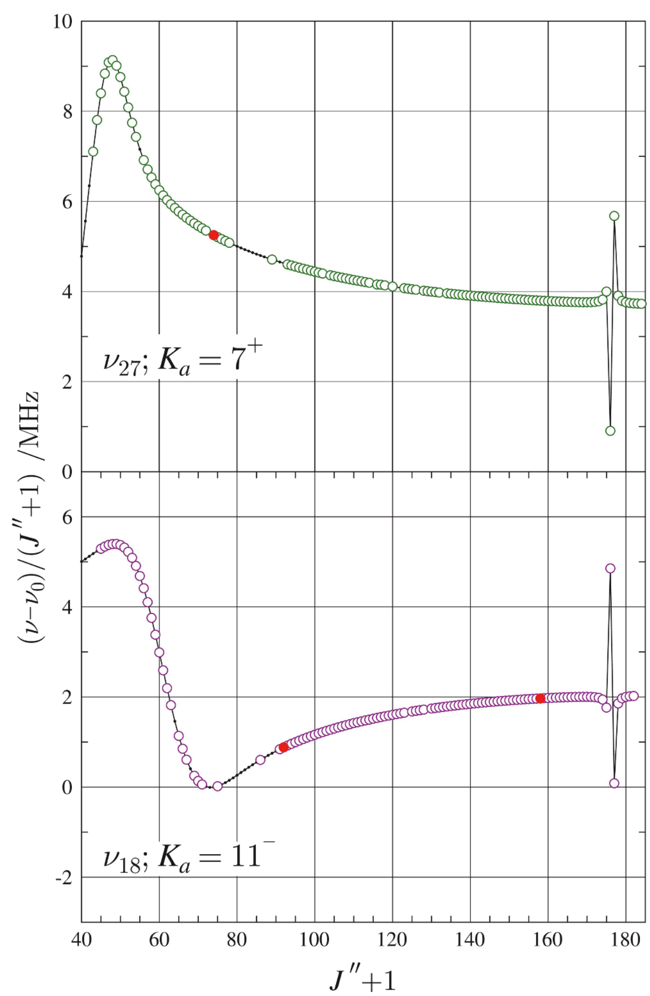

Fig. 8. Resonance plots for 2-cyanopyrimidine showing the $K_a = 11^-$ series for ν_{18} and $K_a = 7^+$ series for ν_{27}. These two resonances conform to the $\Delta K_a = 4$ selection rule for *a*-type resonances. The plotted values are frequency differences between excited-state transitions and their ground-state counterparts, scaled by ($J'' + 1$) in order to make the plots more horizontal. Measured transitions are represented by circles: ν_{18} (magenta), ν_{27} (green). Red circles indicate transitions whose *obs. – calc.* values are more than three times the experimental uncertainty. Predictions from the final coupled fit are represented by a solid black line. (For interpretation of the references to colour in this figure legend, the reader is referred to the web version of this article.)

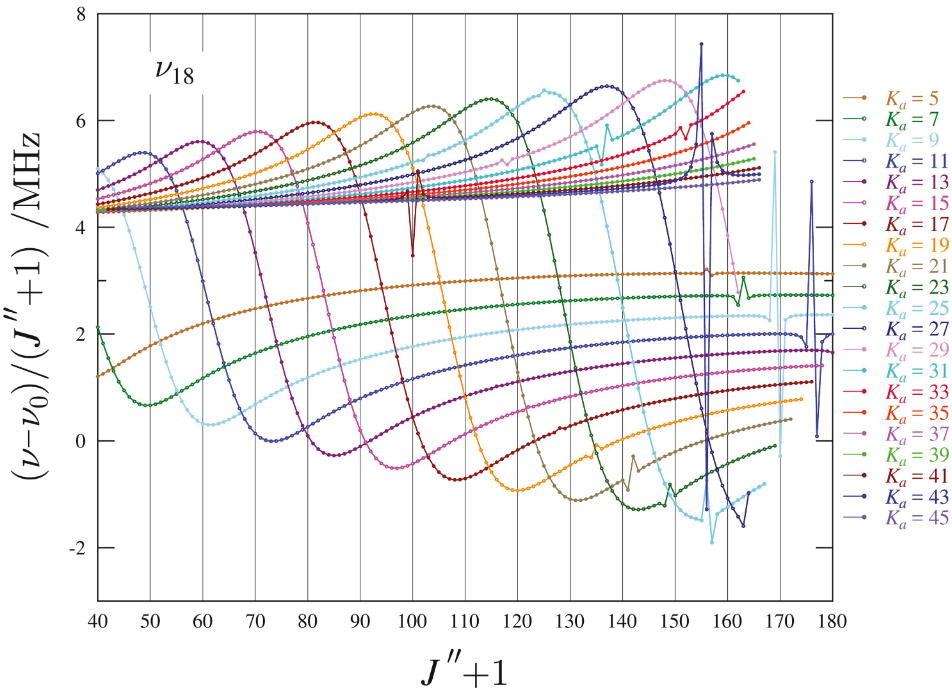

Fig. 9. Superimposed resonance plots of ν_{18} for ${}^{a}R_{0,1}$ odd-K_a^- series from 5 to 45 for 2-cyanopyrimidine. Measured transitions are omitted for clarity, but they are indistinguishable from the plotted values on this scale. The plotted values are frequency differences between excited-state transitions and their ground-state counterparts, scaled by $(J'' + 1)$.

sign between the two vibrational states. The MP2 values of $B_0 - B_v$ and $C_0 - C_v$ are in excellent agreement with the experimental values (within 6%), which provides confidence in the method to determine the vibration–rotation interaction constants. The corresponding B3LYP values are approximately as accurate as the MP2 values for $B_0 - B_v$ and $C_0 - C_v$ (within 7%). In contrast, both the B3LYP and MP2 values of $A_0 - A_v$ show poor agreement with the experimental values, each having similarly large discrepancies and much larger magnitudes than the experimental values (Table 4). The disagreement indicates the presence of untreated Coriolis coupling in both computational results or in the experimental values. The fact that the experimental values are significantly smaller than either computed value suggests that the least-squares fit may be performing a better job of treating the Coriolis coupling. This situation, in which the experimental $A_0 - A_v$ values have different signs than the computed values, was also noted in previous works [17,22]. The average of the computed $A_0 - A_v$ values for ν_{18} and ν_{27} cancels out the unaddressed Coriolis effects, and these averages are in excellent agreement with the experimental average (Table 4). Unsurprisingly, the corresponding average values for the B_v and C_v values are also in excellent agreement between both theoretical treatments and experiment. The $\Delta E_{18,27}$ values for both computational methods are in close agreement; the B3LYP value is approximately 4 cm^{-1} too large and the MP2 value is approximately 2 cm^{-1} too small. The experimental Coriolis $\zeta^{a}_{18,27}$ value is also in satisfactory agreement with both the MP2 and B3LYP values with the experimental value being slightly larger (7%). The agreement between experimental and computational Coriolis $\zeta^{a}_{18,27}$ values, along with a low σ_{fit} value, indicate a satisfactory treatment of the Coriolis coupling that is present in the ν_{18}-ν_{27} dyad of 2-cyanopyrimidine.

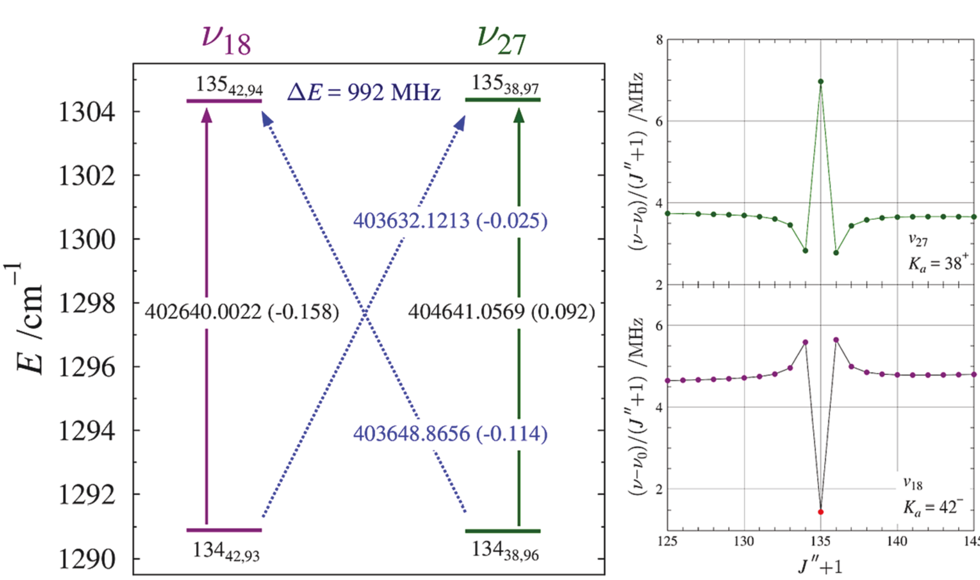

Fig. 10. Energy diagram (left) depicting a representative matched pair of nominal interstate transitions between the ν_{18} (magenta) and ν_{27} (green) vibrational states of 2-cyanopyrimidine. Standard ${}^{a}R_{0,1}$ transitions within vibrational states are denoted by vertical arrows. The diagonal, dashed arrows indicate nominal interstate transitions that are formally forbidden but enabled as a result of rotational energy-level mixing. Values printed on each of the arrows are the corresponding transition frequency (in MHz) with its *obs. – calc.* value in parentheses. The marked energy separation is between the two strongly interacting rotational energy levels. Resonance plots (right) of the K_a series of ν_{18} and ν_{27} show the corresponding resonant intrastate transitions. (For interpretation of the references to colour in this figure legend, the reader is referred to the web version of this article.)

Table 5
Experimental energy separations for selected organic species for the out-of-plane and in-plane nitrile bending modes.

	ΔE_{ip-oop} (cm^{-1})	*ortho* N	*meta* N	*para* N
benzonitrile [12,13]	19.1081701(74)	0	0	0
3-cyanopyridine [15]	15.7524693 (37)	0	1	0
4-cyanopyridine [16]	18.806554 (11)	0	0	1
cyanopyrazine [17]	24.8245962 (60)	1	1	0
cyanopyrimidine (this work)	38.9673191 (77)	2	0	0

The successful incorporation of many resonant and nominal interstate transitions into the data set indicates an adequate treatment of the dyad by the Hamiltonian, since these transitions are highly dependent on $\Delta E_{18,27}$ and the Coriolis-coupling coefficients utilized in the least-squares fit. One example of the state mixing between vibrational states is shown in Fig. 8, where a sharp resonance occurs between the $K_a = 11^-$ series of ν_{18} and $K_a = 7^+$ series of ν_{27} ($\Delta K_a = 4$). The most-perturbed transition, at $J'' + 1 = 176$, is $\sim$ 500 MHz from its unperturbed location. Each of these series also displays large undulations occurring from both global coupling perturbation and centrifugal distortion. The progression of the global undulation, from low to high frequencies as K_a increases, is displayed in Fig. 9. This plot highlights several of the resonances present for the ν_{18}-ν_{27} dyad, and the most perturbed transition, located in $K_a = 43$, is $\sim$ 1 GHz from its unperturbed location. Most resonances are above $J'' + 1 = 130$, reaffirming the utility of the extension of the frequency range to 500 GHz.

A total of 17 independent nominal interstate transitions were measured and incorporated into the least-squares fit, and they were crucial in finalizing several Coriolis-coupling constants and confirming the assignment of some resonant transitions. These nominal interstate transitions occur when rotational energy levels from each vibrational state are close enough in energy that intense state-mixing occurs. In many cases, it is possible to measure corresponding intrastate and interstate transitions for each level to create a matched set of four transitions (Fig. 10). As these four transitions involve the same energy levels, the average of the interstate transition frequencies must be the same as the intrastate transition frequencies. This condition confirms the assignment of all transitions when the difference between the sets of transitions is less than the measurement uncertainty of 50 kHz. The frequency difference between the transitions in Fig. 10 is only 36 kHz despite the higher *obs.* – *calc*. for individual transitions, *e.g.*, the intrastate transition of ν_{18}, where it is one of two transitions in the fit that is greater than three times the measurement uncertainty and is shown in red in the resonance plot of Fig. 10 and in the data distribution plot (Fig. 7). The typical working procedure for least-squares fitting is to scrutinize transitions with greater than two times the measurement uncertainty with regards to including such transitions in the least-squares fit. This transition displays an abnormal line shape, which is likely due to another underlying transition distorting its true frequency. Although this would typically warrant the exclusion of this transition, the very limited number of these important resonant and nominal interstate transitions in the data set make even this imperfectly measured transition highly valuable for the coupling information it provides. As a result, it was retained in the final data set with explicably high error.

Measurement of the precise and accurate value of the energy difference for the out-of-plane and in-plane nitrile bending modes for a variety C(sp^2)–CN-containing organic molecules, including the previously studied cyanoarenes, allows for an analysis of the structural factors that impact the vibrational mode energies. As shown in Fig. 1, the structure of each of the cyanoarenes recently studied in our group [15–17] differs from benzonitrile [12,13] by *N*-atom substitution in the aromatic ring. Similar to benzonitrile, 3-cyanopyridine [15] and 4-cyanopyridine [16] have *ortho* C–H groups adjacent to the nitrile. Cyanopyrazine [17] has an *ortho* C–H group and a nitrogen atom. 2-Cyanopyrimidine from this work completes this series by providing analogous data for a cyanoarene with two *ortho* nitrogen atoms. There is a monotonic increase in the ΔE_{ip-oop} values with increasing substitutions of *ortho* C–H groups with nitrogen atoms shown in Table 5. There is a smaller change to ΔE_{ip-oop} with *meta* substitution in the reverse direction, such that the effects of *ortho* and *meta* substitution are approximately $+10$ and -3 cm^{-1}, respectively.

5. Conclusion

To expand the search for heterocyclic aromatic molecules in the interstellar medium, the current study provides the necessary laboratory data for 2-cyanopyrimidine. The larger dipole moment of 2-cyanopyrimidine (6.5 D) vs pyrimidine (2.3 D) increases the possibility of detection in the ISM if these species were to have similar abundances. The combination of the spectroscopic constants provided here, along with computed (provided in Supplementary Material) or experimental nuclear quadrupole coupling constants, would reliably predict transition frequencies much lower or slightly higher in frequency than the frequency range of the current measurements (130–500 GHz). The least-squares fit of the Coriolis-coupled dyad of ν_{18} and ν_{27} allows for a precise determination of the energy separation of the fundamental modes, $\Delta E_{18,27}$, although high-resolution infrared spectroscopy is needed to determine the fundamental frequencies. This infrared study would be challenging, however, since ν_{18} and ν_{27} have quite low predicted intensities (0.1 and 0.6 km/mol (MP2), respectively). Of the cyanoarenes studied to date, 2-cyanopyrimidine exhibits the largest energy difference for the out-of-plane and in-plane nitrile bending modes (ΔE_{ip-oop} = 38.9673191 (77) cm^{-1}). This large energy separation notwithstanding, a two-state Hamiltonian is required to adequately address the transition frequencies observed for each vibrational state – even in the 130 – 360 GHz range. At the same time, highly-perturbed transition frequencies (resonances) above 360 GHz are required to adequately describe the Coriolis perturbation and obtain a satisfactory least-squares fit. This behavior demonstrates how broadly Coriolis perturbation can affect transition frequencies, even those that are not "highly" perturbed as resonances, and that the resonant transitions provide important constraints on the determination of the spectroscopic parameters that cannot be obtained from transition frequencies influenced by the global Coriolis interaction alone.

Declaration of Competing Interest

The authors declare that they have no known competing financial interests or personal relationships that could have appeared to influence the work reported in this paper.

Data availability

Data are provided in the article and in the Supplementary Material.

Acknowledgments

We gratefully acknowledge funding from the U.S. National Science Foundation for support of this project (CHE-1954270). We thank Michael McCarthy for the loan of an amplification-multiplication chain and the Harvey Spangler Award (to B.J.E) for support of the purchase of the corresponding zero-bias detector.

Appendix A. Supplementary material

Supplementary data to this article can be found online at https://doi.org/10.1016/j.jms.2023.111737.

References

[1] J. Cernicharo, A.M. Heras, A.G.G.M. Tielens, J.R. Pardo, F. Herpin, M. Guélin, L.B. F.M. Waters, Infrared Space Observatory's Discovery of C_4H_2, C_6H_2, and Benzene in CRL 618, Astrophys. J. 546 (2001) L123–L126.

[2] T.J. Barnum, M.A. Siebert, K.L.K. Lee, R.A. Loomis, P.B. Changala, S.B. Charnley, M.L. Sita, C. Xue, A.J. Remijan, A.M. Burkhardt, B.A. McGuire, I.R. Cooke, A Search for Heterocycles in GOTHAM Observations of TMC-1, J. Phys. Chem. A 126 (2022) 2716–2728.

[3] M.L. Kutner, D.E. Machnik, K.D. Tucker, R.L. Dickman, Search for interstellar pyrrole and furan, Astrophys. J. 242 (1980) 541–544.

[4] Y.-J. Kuan, C.-H. Yan, S.B. Charnley, Z. Kisiel, P. Ehrenfreund, H.-C. Huang, A search for interstellar pyrimidine, Mon. Not. R. Astron. Soc. 345 (2003) 650–656.

[5] S.B. Charnley, Y.-J. Kuan, H.-C. Huang, O. Botta, H.M. Butner, N. Cox, D. Despois, P. Ehrenfreund, Z. Kisiel, Y.-Y. Lee, A.J. Markwick, Z. Peeters, S.D. Rodgers, Astronomical searches for nitrogen heterocycles, Adv. Space Res. 36 (2005) 137–145.

[6] J. Basha N, N.M. Goudgaon, A comprehensive review on pyrimidine analogs-versatile scaffold with medicinal and biological potential, J. Mol. Struct. 1246 (2021) 131168.

[7] M.N. Simon, M. Simon, Search for Interstellar Acrylonitrile, Pyrimidine, and Pyridine, Astrophys. J. 184 (1973) 757–762.

[8] H.S.P. Müller, S. Thorwirth, D.A. Roth, G. Winnewisser, The Cologne Database for Molecular Spectroscopy, CDMS, Astron. Astrophys. 370 (2001) L49–L52.

[9] H.S.P. Müller, F. Schlöder, J. Stutzki, G. Winnewisser, The Cologne Database for Molecular Spectroscopy, CDMS: a Useful Tool for Astronomers and Spectroscopists, J. Mol. Struct. 742 (2005) 215–227.

[10] B.A. McGuire, A.M. Burkhardt, S.V. Kalenskii, C.N. Shingledecker, A.J. Remijan, E. Herbst, M.C. McCarthy, Detection of the Aromatic Molecule Benzonitrile (*c*-C_6H_5CN) in the Interstellar Medium, Science 359 (2018) 202–205.

[11] B.A. McGuire, R.A. Loomis, A.M. Burkhardt, K.L.K. Lee, C.N. Shingledecker, S. B. Charnley, I.R. Cooke, M.A. Cordiner, E. Herbst, S. Kalenskii, M.A. Siebert, E. R. Willis, C. Xue, A.J. Remijan, M.C. McCarthy, Detection of two interstellar polycyclic aromatic hydrocarbons via spectral matched filtering, Science 371 (2021) 1265–1269.

[12] M.A. Zdanovskaia, B.J. Esselman, H.S. Lau, D.M. Bates, R.C. Woods, R.J. McMahon, Z. Kisiel, The 103–360 GHz rotational spectrum of benzonitrile, the first interstellar benzene derivative detected by radioastronomy, J. Mol. Spectrosc. 351 (2018) 39–48.

[13] M.A. Zdanovskaia, M.-A. Martin-Drumel, Z. Kisiel, O. Pirali, B.J. Esselman, R. C. Woods, R.J. McMahon, The eight lowest-energy vibrational states of benzonitrile: analysis of Coriolis and Darling-Dennison couplings by millimeter-wave and far-infrared spectroscopy, J. Mol. Spectrosc. 383 (2022), 111568.

[14] P.M. Dorman, B.J. Esselman, R.C. Woods, R.J. McMahon, The 130 to 500 GHz rotational spectrum of 2-cyanopyridine (*o*-C_5H_4N-CN), manuscript in preparation (2023).

[15] P.M. Dorman, B.J. Esselman, R.C. Woods, R.J. McMahon, An analysis of the rotational ground state and lowest-energy vibrationally excited dyad of 3-cyano-pyridine: Low symmetry reveals rich complexity of perturbations, couplings, and interstate transitions, J. Mol. Spectrosc. 373 (2020), 111373.

[16] P.M. Dorman, B.J. Esselman, J.E. Park, R.C. Woods, R.J. McMahon, Millimeter-wave spectrum of 4-cyanopyridine in its ground state and lowest-energy vibrationally excited states, ν_{20} and ν_{30}, J. Mol. Spectrosc. 369 (2020), 111274.

[17] B.J. Esselman, M.A. Zdanovskaia, H.H. Smith, R.C. Woods, R.J. McMahon, The 130–500 GHz Rotational Spectroscopy of Cyanopyrazine ($C_4H_3N_2$-CN), J. Mol. Spectrosc. 389 (2022), 111703.

[18] S. Doraiswamy, S.D. Sharma, Microwave spectrum of 2-cyanopyridine, Curr. Sci. 40 (1971) 398–399.

[19] R.G. Ford, The microwave spectra and dipole moments of the cyanopyridines, J. Mol. Spectrosc. 58 (1975) 178–184.

[20] N. Heineking, H. Dreizler, Nuclear Quadrupole Coupling Effects in the Rotational Spectrum of 4-Cyanopyridine, Z. Naturforsch. A 42 (1987) 83–86.

[21] N. Vogt, K.P.R. Nair, J.-U. Grabow, J. Demaison, Microwave rotational spectrum and ab initio computations on 4-cyanopyridine: molecular structure and hyperfine interactions, Mol. Phys. 116 (2018) 3530–3537.

[22] H.H. Smith, S.M. Kougias, B.J. Esselman, R.C. Woods, R.J. McMahon, Synthesis, Purification, and Rotational Spectroscopy of 1-Cyanocyclobutene (C_5H_5N), J. Phys. Chem. A 126 (2022) 1980–1993.

[23] B.J. Esselman, S.M. Kougias, M.A. Zdanovskaia, R.C. Woods, R.J. McMahon, Synthesis, Purification, and Rotational Spectroscopy of (Cyanomethylene) Cyclopropane—An Isomer of Pyridine, J. Phys. Chem. A 125 (2021) 5601–5614.

[24] Z. Kisiel, M.-A. Martin-Drumel, O. Pirali, Lowest vibrational states of acrylonitrile from microwave and synchrotron radiation spectra, J. Mol. Spectrosc. 315 (2015) 83–91.

[25] G. Cazzoli, Z. Kisiel, The rotational spectrum of acrylonitrile in excited states of the two low-frequency CCN bending vibrational modes, J. Mol. Spectrosc. 130 (1988) 303–315.

[26] B.K. Amberger, B.J. Esselman, J.F. Stanton, R.C. Woods, R.J. McMahon, Precise Equilibrium Structure Determination of Hydrazoic Acid (HN_3) by Millimeter-wave Spectroscopy, J. Chem. Phys. 143 (2015), 104310.

[27] B.J. Esselman, B.K. Amberger, J.D. Shutter, M.A. Daane, J.F. Stanton, R.C. Woods, R.J. McMahon, Rotational Spectroscopy of Pyridazine and its Isotopologs from 235–360 GHz: Equilibrium Structure and Vibrational Satellites, J. Chem. Phys. 139 (2013), 224304.

[28] Z. Kisiel, L. Pszczółkowski, I.R. Medvedev, M. Winnewisser, F.C. De Lucia, E. Herbst, Rotational spectrum of *trans–trans* diethyl ether in the ground and three excited vibrational states, J. Mol. Spectrosc. 233 (2005) 231–243.

[29] H.M. Pickett, Determination of collisional linewidths and shifts by a convolution method, Applied Optics 19 (1980) 2745–2749.

[30] H.M. Pickett, The fitting and prediction of vibration-rotation spectra with spin interactions, J. Mol. Spectrosc. 148 (1991) 371–377.

[31] Z. Kisiel, Assignment and Analysis of Complex Rotational Spectra, in: J. Demaison, K. Sarka, E.A. Cohen (Eds.), Spectroscopy From Space, Springer, Netherlands, Dordrecht, 2001, pp. 91–106.

[32] Z. Kisiel, PROSPE - Programs for ROtational SPEctroscopy. http://info.ifpan.edu.pl/~kisiel/prospe.htm.

[33] M.J. Frisch, G.W. Trucks, H.B. Schlegel, G.E. Scuseria, M.A. Robb, J.R. Cheeseman, G. Scalmani, V. Barone, G.A. Petersson, H. Nakatsuji, X. Li, M. Caricato, A.V. Marenich, J. Bloino, B.G. Janesko, R. Gomperts, B. Mennucci, H.P. Hratchian, J.V. Ortiz, A.F. Izmaylov, J.L. Sonnenberg, Williams, F. Ding, F. Lipparini, F. Egidi, J. Goings, B. Peng, A. Petrone, T. Henderson, D. Ranasinghe, V.G. Zakrzewski, J. Gao, N. Rega, G. Zheng, W. Liang, M. Hada, M. Ehara, K. Toyota, R. Fukuda, J. Hasegawa, M. Ishida, T. Nakajima, Y. Honda, O. Kitao, H. Nakai, T. Vreven, K. Throssell, J.A. Montgomery Jr., J.E. Peralta, F. Ogliaro, M.J. Bearpark, J.J. Heyd, E.N. Brothers, K.N. Kudin, V.N. Staroverov, T.A. Keith, R. Kobayashi, J. Normand, K. Raghavachari, A.P. Rendell, J.C. Burant, S.S. Iyengar, J. Tomasi, M. Cossi, J.M. Millam, M. Klene, C. Adamo, R. Cammi, J.W. Ochterski, R.L. Martin, K. Morokuma, O. Farkas, J.B. Foresman, D.J. Fox, Gaussian 16 Rev. C.01. Wallingford, CT, 2016.

[34] J.R. Schmidt, W.F. Polik, WebMO Enterprise. 17.0.012e ed.; WebMO, LLC., Holland, MI, USA, 2017.

[35] M.A. Zdanovskaia, B.J. Esselman, R.C. Woods, R.J. McMahon, The 130–370 GHz rotational spectrum of phenyl isocyanide (C_6H_5NC), J. Chem. Phys. 151 (2019), 024301.